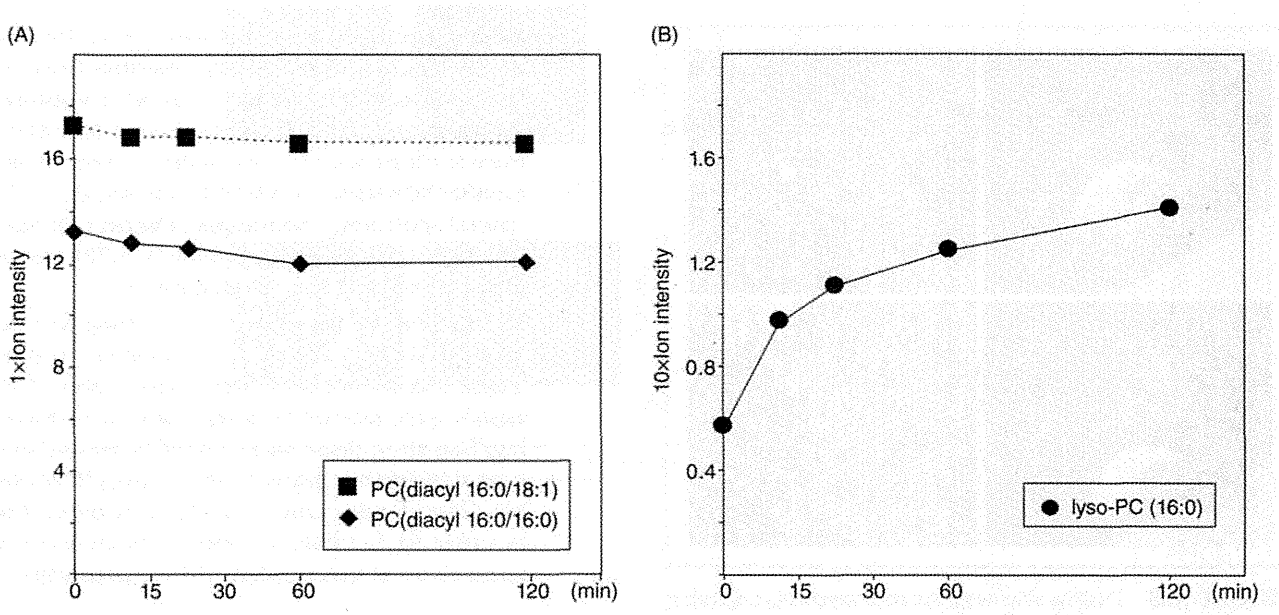

FIGURE 3.27 Postmortem degradation of GPLs observed by IMS. GPLs were degraded within 15 min in a series of mouse brains extracted at different times (15, 30, 60, and 120 min) (A). Conversely, lyso-PC was increased during the period (B) [64,65].

TABLE 3.5 The Major Cautionary Points at Each Step of Slice Preparation

Procedure for Preparing a Frozen Section for IMS
Tissue extraction
Because of rapid metabolic turnover, tissues should be handled in a fixed time course, particularly for the analysis of small molecules.
↓
Embedding
Avoid the use of polymeric compounds, such as optimum cutting temperature (OCT) compound, for embedding [4,10]. As an alternative, a precooled semiliquid gel of 2% sodium carboxymethylcellulose (CMC) can be used as an embedding compound, as it does not interfere with MS [63].
↓
Sectioning
Tissue thickness < 20 μm improves spectrum quality [66].
↓
Mounting
The use of conductive materials is recommended for supporting the tissue section [91][a].
↓
Washing
By removing small molecules such as lipids, the tissue-washing process improves the spectrum quality for protein/peptide detection [9–11].
↓
Drying
Failure to dry sections sufficiently may cause samples to peel off in the vacuum chamber of the mass spectrometer.
↓
Sputtering
Sputtering of metals (e.g., gold) onto tissue sections before/after the matrix application process improves the spectrum quality [63,72].

[a] Some instruments support the use of nonconductive materials [1].

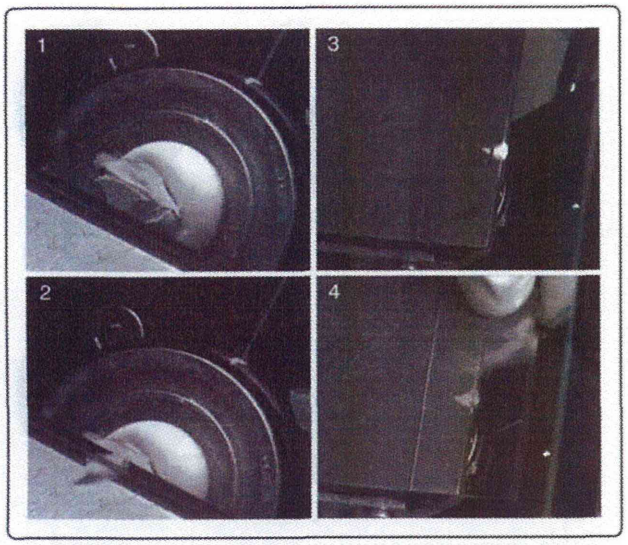

FIGURE 3.28 Cutting thin sections with cryostat. 1. Cutting tissues into optimal tissue thickness. 2. Keep the slice under the antiroll for a while, until it no longer curls. 3 and 4.Put the indium tin oxide (ITO)-coated glass slides into the chamber, immediately place the slides over the tissue slice, and paste tissues on it.

mass spectra would virtually mask the analyte signal. This virtually hides all of the smaller peaks (Figure 3.29B). For this reason, when preparing sections for IMS, OCT is used only to "support" the tissue blocks and, thus, OCT does not directly attach to the tissue being analyzed. As an alternative, a precooled semiliquid gel of 2% sodium CMC can be used as an embedding compound that does not interfere with MS [63].

2. Slice thickness is the most important factor associated with IMS measurement. When the thickness of a slice is >15 μm, the sensitivity deteriorates, particularly when high molecular weight proteins are analyzed [66] (Figure 3.30). This difference can be attributed to a phenomenon referred to as the "charging effect" [67]. Generally, biological tissue sections have low intrinsic electric conductivity, and this tendency is considered more apparent with thicker tissue sections. In this state, a surplus electric charge generated by laser irradiation is not lost through the sample stage. Thus, multiple charged ions are generated—and ultimately leads to a significant loss of sample ions that would otherwise reach the detector [67]. However, a high technical proficiency is required in order to prepare slices with thicknesses of several micrometers each. Currently, most samples are prepared with a slice thickness of 10–20 μm [68,69]. These medium-thick sections appear to provide a good compromise between optimal IMS performance and experimental efficiency [70], particularly when a large number of samples need to be analyzed [71]. The "metal sputtering" technique enhances the signal intensity and thus image quality [63,72], presumably by avoiding the "charging effect."
3. Dehydration of tissue sections for long times can lead to altered signals [73]. Goodwin and colleagues demonstrated that, even within 1 min, signals were altered, both increasing and decreasing. Therefore, tissue slices should be moved to the next step (matrix application) as quickly as possible. Considerable care is required at these stages in order to facilitate a comparison between the biomarkers in independent IMS experiments.

3.3.2.3 Spray-Coating of the Matrix Solution with an Artistic Airbrush Among the several matrix application methods, the spray-coating method is one of the frequently used methods. In this process, an entire tissue section can be coated with relatively small crystals homogenously. For this operation, several instruments, including TLC sprayers and artistic airbrushes, are available.

To achieve optimal spraying: (1) minimize the droplet size, to accelerate the dry rate, (2) keep the airbrush in a position at same distance from tissue, and (3) gradually move the airbrush horizontally. Further technical tip to bear in mind when executing this method is to maintain equilibrium between the two rates—one rate, at which a fine aerosol of airbrushed matrix solution slightly moisturizes the tissue section which facilitates analyte extraction, and the other rate, at which the quick solvent evaporates which prevent analyte migration (Figure 3.31 inset). To execute this, important parameters to care for practical spraying include (1) the size of the droplet, (2) the amount of the mist, (3) the angles and distances between the spray nozzle and the tissue section, and (4) laboratory temperature and humidity. These parameters are described below in detail.

Preparation of Matrix Solution

1. Weigh appropriate amount of matrix compound and put it into an organic solvent-tolerant microtube.
2. Add 1.0 mL of solvent with organic solvent-tolerant pipette tips.
3. Dissolve the matrix compound thoroughly by vortexing or performing brief sonication.
4. Store at room temperature until use.

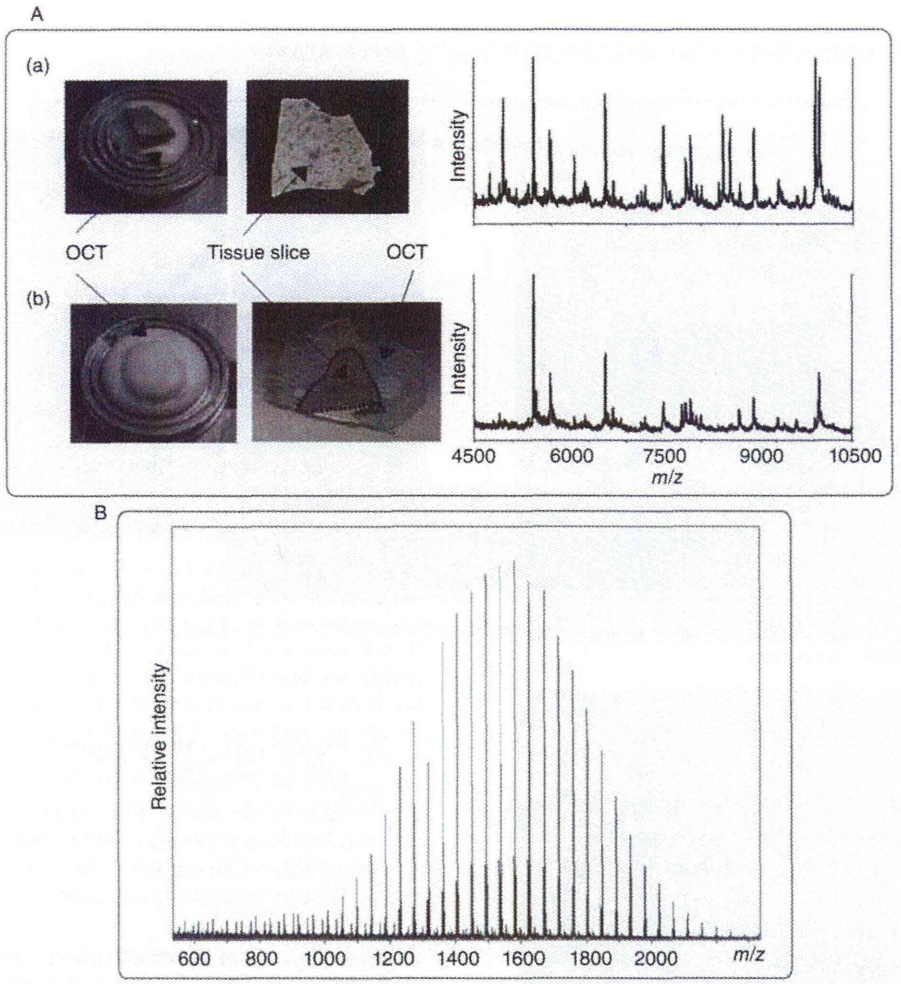

FIGURE 3.29 Residual OCT polymer on the tissue slices degrades the mass spectra. A. Decrease in detection sensitivity of the ions originating from proteins due to contamination with OCT. OCT adhering to the tissue section diminishes the detectable peaks. (a) A case in which OCT was used only for supporting the tissue block. (b) A case in which the tissue block was completely embedded with OCT. B. Contamination with OCT leads to the presence of extremely high polymer peaks.

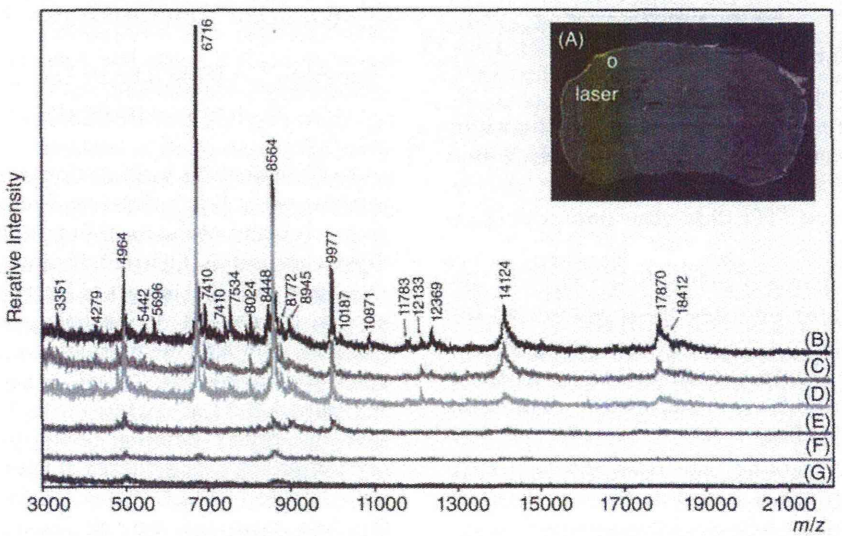

FIGURE 3.30 Mass spectra obtained from the cerebral cortex region [66]. The mass spectra obtained from the cerebral cortex region in mouse brain slices (a white circle in (A) with thicknesses of 2 μm (B), 5 μm (C), 10 μm (D), 15 μm (E), 30 μm (F), and 40 μm (G). A larger number of mass peaks with high signal-to-noise (S/N) ratios were observed in the spectra obtained from sections with 2, 5, and 10 μm thicknesses than in those obtained from sections with 15, 30 and 40 μm thicknesses.

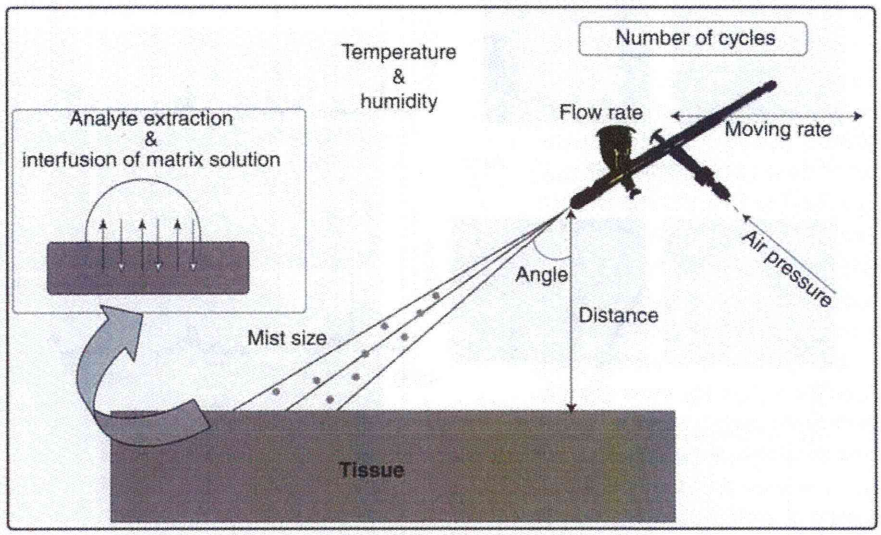

FIGURE 3.31 Representative parameters of spraying operation with an airbrush, required to be controlled among the trials for the reproducible IMS experiment.

Notes:

- Microtubes with organic solvent-tolerant properties can be purchased from Eppendorf Co., Ltd.
- Use HPLC or LC/MS-grade solvent for preparing matrix solution.
- Preparing the matrix solution on the day of experiment is recommended.

Matrix Application Using an Airbrush

1. Pour approximately 1.0 mL of the solvent for the matrix solution into the airbrush.
2. Optimize the size of the droplet, the amount of mist, and the angles and distances between the nozzle and the sample.
3. Remove the solvent from the airbrush.
4. Mask the areas outside of the tissue section, which is mounted on the ITO slide glass, with a masking tape.
5. Fix the masked ITO slide glass onto a perpendicular board.
6. Pour the prepared matrix solution into the airbrush and spray onto the tissue section on the ITO slide glass.
7. As a rough guide for optimal coating, spray approximately 0.5–1.0 mL of matrix solution for one ITO slide glass.
8. Remove the masking tape from the ITO slide glass after spraying, and place the sample in an airtight container with dry silica gel.
9. Perform the IMS measurement as soon as possible to minimize the progress of sample damage.
10. Figure 3.32 shows an example of good and unfavorable spraying results by spraying DHB matrix solution (50 mg/mL, 70% MeOH containing 10 mM potassium acetate).

3.3.2.4 Spectrum Normalization In the data analysis of MALDI-IMS, experimenters should not interpret peak intensities of each metabolite simply as metabolite concentrations. Dr. R. Murphy explained this issue using a following equation. Observed ion intensities were result of not only metabolite concentration, but also functions of ionization efficiency of each metabolite compound and local environmental factors [74]:

$$\text{Intensity}_{m/z} = f([\text{metabolite conc.}]\times[\text{ionization cross-section}]\times[\text{local environment}]\times\ldots).$$

In this equation, local environmental factors include analyte extraction efficiency from the distinct tissue structures, and as the most important factor, the matrix crystal condition. Figure 3.33 shows scanning electron microscope (SEM) images of DHB crystals on the tissue section as a result of manual spraying of the matrix solution. Although the presented manual spraying result could be classified into "good" example (like that shown in Figure 3.31A), as can been seen, the SEM observation revealed rather heterogeneous distribution of DHB crystals on the tissue surface. If tissue surface is scanned with a typical MALDI laser, there could be "hot spot" in which more ions were detected than other location,

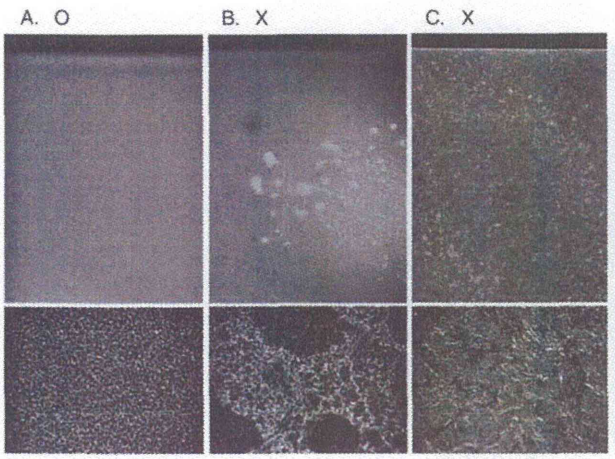

FIGURE 3.32 Result examples of DHB spray coating with the airbrush [41]. A. A properly handled spray-coating step created a uniform matrix crystal layer, and awareness of certain technical points leads to a successful coating step. B. Too small a distance between the airbrush and the tissues (<10 cm) often creates large droplets of matrix solution and results in inhomogeneous crystals. C. Humidity is also an important factor. Room humidity was held under 25% at room temperature (25°C). High humidity tends to cause formation of needle-like crystals (>80%, at room temperature). The upper panel shows stereoscopic microscope images, and the lower panel shows phase-contrast microscopic images of the matrix layer formed on the glass slides.

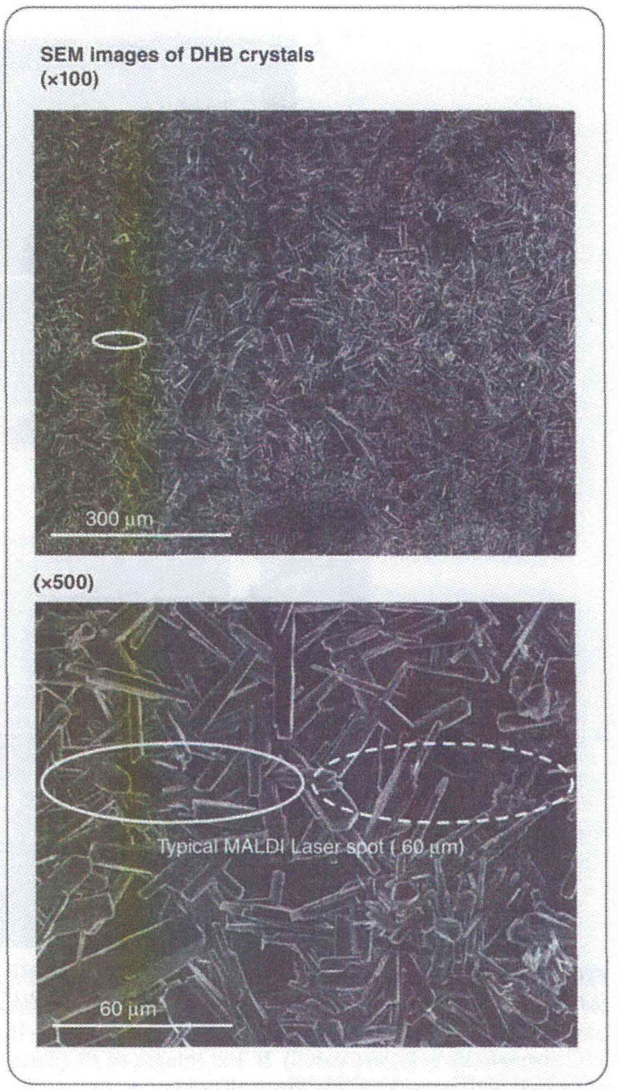

FIGURE 3.33 Size comparison of DHB crystal and typical MALDI-laser spot. DHB solution was sprayed onto the mouse brain section and the crystals were observed by SEM. The white ellipse represents the typical size of MALDI laser spot. Each matrix crystals typically have 20–60 μm length, and they did not distribute heterogeneously on the tissue surface.

and it in turn results in spot-to-spot variance of signal intensities [75,76].

This problem was at least partially solved using a spectrum-normalization procedure with total ion current (TIC) (Figure 3.33). We previously studied the effectiveness of spectrum normalization with TIC; the obtained spectra were multiplied with arbitrary variables such that all spectra had equal TIC values (i.e., equal integral values of the measured m/z region [m/z 400–900]). Such TIC normalization is available with the "Normalize Spectra" function of FlexImaging 2.0 software (Bruker Daltinics) with filter function to exclude a number of noise spectra from the normalization process (see details in the software manual).

To evaluate the effect of the normalization procedure, we prepared a section of mouse brain homogenate that had a uniform distribution of biomolecules. Figure 3.34A shows the ion images for m/z 772.6 corresponding to PC(diacyl-16:0/16:0), with and without spectrum normalization. After the normalization procedure, the image was corrected such that the ion distribution was uniform throughout the section. The signal intensity was then plotted and found to have a Gaussian distribution. Spectrum normalization with TIC improved the results of the IMS of mouse brain sections. Figure 3.34B shows the ion images of a mouse brain section for PC(diacyl-16:0/16:0), with and without spectrum normalization. In the ion image without normalization, the ion distribution was heterogeneous, even between adjacent pixels. Furthermore, the signal intensity was found to decrease with time (arrowhead). In contrast, when the normalization procedure was used, a clear ion-distribution pattern that correlated well with the anatomical features of the brain section was obtained [41].

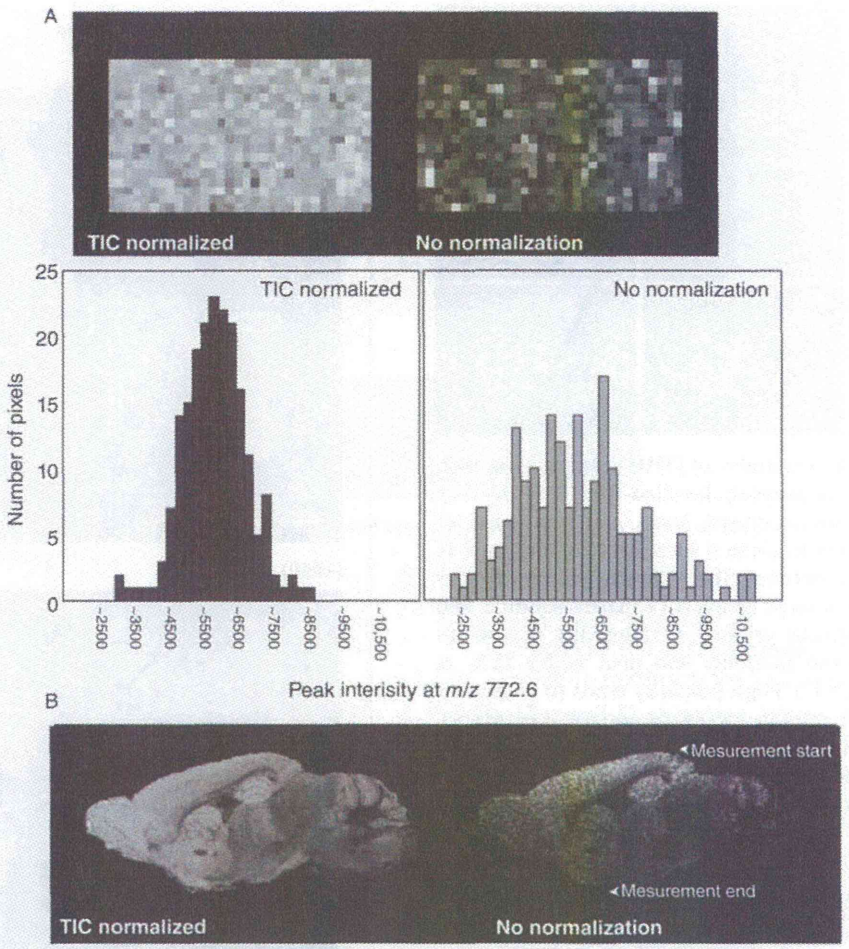

FIGURE 3.34 Spectrum normalization using TIC improves both the quantitative ability and visualization quality of IMS. A. IMS results for PC(diacyl-16:0/16:0) on a section of mouse brain homogenate, processed with or without TIC normalization (upper panel), and plot of ion intensity distribution for PC(diacyl-16:0/16:0) obtained from a brain homogenate section, with or without TIC normalization (lower panel). B. Ion images of PC(diacyl-16:0/16:0) on an adult mouse brain section, in which spectra were processed with or without TIC-normalization.

Another way of the spectrum normalization is using an external standard (ES) compound spiked in the matrix solution. We have also studied this normalization method for phospholipid imaging; the methylcarbamyl platelet-activating factor (C-PAF) (C-16) was used as the ES compound by considering the following two criteria: (1) no other mass peaks overlap the peak of the ES compound and (2) the ES compound has sufficient ionization capability on the tissue section, in which numerous biological compounds compete to ionize. All obtained spectra were multiplied to equalize the intensity of the ES and such normalization produces improved ion images of biomolecules by eliminating the variations in ionization efficiency.

First, we determined the optimal concentration of C-PAF for spectrum normalization. The spectra were normalized so that the C-PAF peaks at *m/z* 561.4 have equal intensities during the normalizing process. Figure 3.35A shows the ion images of C-PAF (*m/z* 561) with and without spectrum normalization. Regarding the brain section sprayed with the matrix solution containing 0.5, 5, and 25 mg/mL of C-PAF, spectrum normalization could not be performed successfully at some data points because of insufficient intensity of the ES peak, since mass peaks with insufficient intensity of C-PAF could not be recognized by the software as ES peaks. On the other hand, successful normalization was achieved for the section sprayed with 50 mg/mL of C-PAF, since ion signals of C-PAF equalized among the data points.

Figure 3.35B shows the ion images of PC(diacyl-16:0/18:1) (*m/z* 782) with and without spectrum normal-

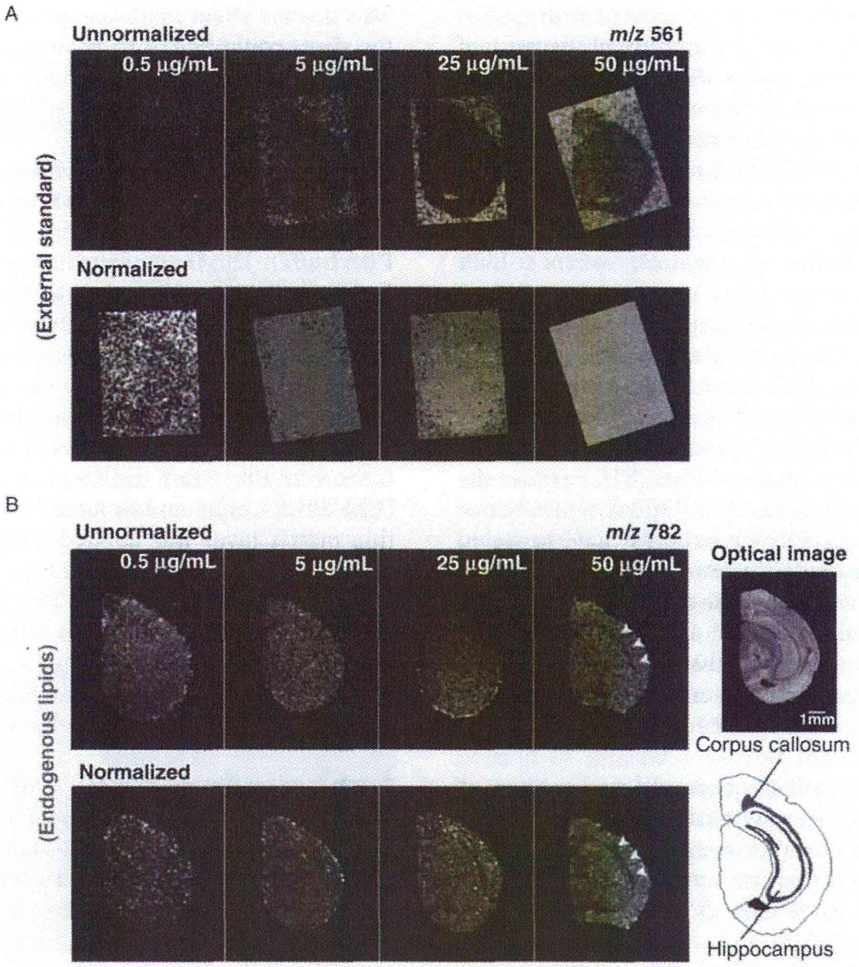

FIGURE 3.35 Comparison of unnormalized and normalized ion images. These images are successive mouse coronal brain sections. The ion at *m/z* 561 is derived from ES and *m/z* 782 is derived from PC(diacyl-16:0/18:1).

ization. While the inner structure of the brain such as the hippocampus region could not be distinguished in the unnormalized ion images, normalized images (50 mg/mL of C-PAF) showed a clear borderline of the hippocampus, indicated by the absence of PC (diacyl-16:0/18:1) in the corpus callosum (arrowheads). The normalization process with C-PAF clearly improved the ion distribution images, providing sharply defined tissue edges and increased dynamic range.

3.4 STATISTICAL PROCEDURES FOR IMS DATA ANALYSIS

3.4.1 MALDI-IMS with Statistical Analyses Revealed Abnormal Distribution of Metabolites in Colon Cancer Liver Metastasis

In the following chapter, a medical application of MALDI-IMS to colon cancer liver metastasis with use of the presented procedures is described. In addition to the shown procedures, here we employed statistical procedure for efficient analysis of complex IMS data sets. The goal of this study is to discover potential biomarkers which are specifically found in normal or diseased cells.

The IMS capability to simultaneously detect multiple metabolites at a time, even with spatial information, facilitates this emerging technique as an effective tool for biomarker discovery, within surgically resected tissues. In fact, a previous study has shown that IMS can discriminate cancer types (such as primary or nonprimary cancer) based on their molecular signature, and can even predict survival rate among human patients [77]. For this kind of purpose, it is necessary to utilize statistical analyses to extract useful information from enormous IMS data sets. The MS of tissues gives an extremely complex spectrum with hundreds of to a thousand peaks obtained from a single data point, and

furthermore, several thousands of spectra with spatial data are obtained at one IMS measurement. Because of the complexity and enormousness of the IMS data set, for discovery of biomarkers, manual processing of the data set in order to obtain significant information is not a realistic procedure. In this regard, today, multivariate analysis becomes a powerful tool in IMS data analysis. Here, we applied the statistical procedure to the IMS results of the pathological specimen, colon cancer liver metastasis.

Colon cancer is a challenging worldwide clinical problem and the incidence rate of colon cancer has been rising rapidly in Japan [78]. Genealogy is known to be a risk factor [79] and as environmental factors, aging [80] and diet, particularly a high intake of animal protein and fat along with a low intake of fiber [81], increase the incidence of colorectal cancer. Until today, a number of approaches including a cDNA microarray have revealed characteristics of cancer cells with some success, such as the discovery of specific gene expressions for drug resistance [82]. In addition to this, IMS approaches presented here which enable comprehensive analysis of metabolite expression patterns in tissues might improve our ability to understand the molecular complexities of tumor cells.

In this chapter, we will show altered composition of metabolites in the cancerous tissue revealed by IMS, with both manual data processing and statistical data management. In particular, as a statistical strategy, an unsupervised multivariate data analysis technique that enables us to sort the data sets without any reference information is described. A major method that is related to IMS, namely principal component analysis (PCA), will be described in detail.

3.4.2 Materials and Methods

3.4.2.1 Chemicals TFA was purchased from Merck (Darmstadt, Germany). Methanol was purchased from Wako Pure Chemical Industries (Osaka, Japan). 2,6-dihydroxy acetophenone (2,6-DHA) was purchased from Bruker Daltonics. A calibration standard for the low *m/z* region was prepared by mixing angiotensin III ($[M+H]^+$: 899.47) and Leu-Euk ($[M+H]^+$: 556.28). All the chemicals used in this study were of the highest purity available.

3.4.2.2 Conductive Sheet The conductive sheet was purchased from Tobi Co., Ltd. (Osaka, Japan). This sheet has a thin ITO layer on a polyethylene terephthalate. The sheet was 125 μm thick and its conductivity was 100 Ω. The transparency was 80% ($\lambda = 550$ nm), so that we could observe stained tissues with transmitted light. This flexible sheet made sample handling easy, because the sheet could be cut to an arbitrary size with a paper cutter and samples did not crack easily, which was sometimes problematic with glass slides.

3.4.2.3 Tissue Block Preparation A tissue block with colon cancer liver metastasis was removed from a Japanese patient during an operation, and rinsed with PBS buffer. The tissue was then immediately frozen in liquid nitrogen to minimize degradation, and was kept at −80°C. Informed consent was obtained before the operation.

3.4.2.4 Sample Preparation Before sectioning, the liver block was left for 30 min at −20°C. The tissue sections were sliced to a thickness of 3 μm using a cryostat (CM 3050; Leica) and mounted onto the ITO sheet. A thin matrix layer was applied to the surface by an air-brush. A 2-min spraying of 2,6-DHA solution (30 mg/mL in 70% methanol/0.1% TFA) was iterated twice. During spraying, the distance between the nozzle and the tissue surface was kept at 15 cm. After drying, the ITO sheet was attached to a metal-coated glass slide by conductive tape to facilitate electrical conduction.

3.4.2.5 Conditions of MS and MALDI-IMS The tissue section was analyzed using a matrix-assisted laser desorption/ionization time-of-flight mass spectrometry (MALDI-TOF)/time of flight (TOF)-type instrument, Ultraflex II TOF/TOF (Bruker Daltonics), which was equipped with a Nd:YAG laser with a 200 Hz repetition rate. External calibration solution was deposited on the surface of the ITO sheet to minimize mass shift. In this experiment, an acceleration voltage was set to 25 kV.

3.4.2.6 IMS A raster scan on the tissue surface was performed automatically. Laser irradiation consisted of 100 shots in each spot. The interval of data points was 100 μm, giving a total of 445 data points in the tissue section. The spectra shown in the results section were accumulated in square sections (300×300 μm) of normal and cancerous areas. Here, we did not apply data processing such as smoothing or baseline subtraction. The reconstructions from the spectra were performed by FlexImaging (Bruker Daltonics).

3.4.2.7 Statistical Analysis Statistical analyses were carried out using the ClinProTools 2.2 Software (Bruker Daltonics). For the statistical analyses, the mass spectra were internally recalibrated on common peaks (also known as spectral alignment) and normalized on the TIC. An average spectrum created from all single spectra was used for a peak picking and to define integration ranges. These integration ranges were used to

obtain the intensities or areas on the single spectra. The signal intensities were used for all calculations.

3.4.3 Results and Discussion

3.4.3.1 Comparison of Averaged Mass Spectra in Normal and Cancerous Areas At first, a tissue section with colon cancer liver metastasis was stained with HE for histological observation (Figure 3.36a). The histochemical staining enables us to distinguish the normal, stroma, and cancer cells which were localized on the left, middle, and right locations of the tissue section, respectively. A successive tissue section was used for MALDI-IMS and after the measurement, according to the histological observation, two quadrate areas—one from the normal area and the other from the cancerous area—were selected to collect and average the obtained mass spectra (Figure 3.36b).

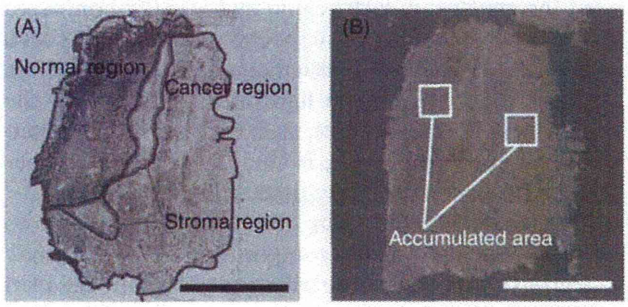

FIGURE 3.36 Histological observation of HE-stained liver tissue section with colon cancer metastasis. A. The HE-stained section allows us to distinguish the normal, stroma, and cancer cells which were localized on the left, middle, and right locations of the section, respectively. B. Photograph of the tissue section prepared for MALDI-IMS. From the data points in white squares represented in B, mass spectra were collected and averaged. Bars: 1 mm.

Figure 3.37 shows the averaged mass spectra from the cancerous (Figure 3.37a) and normal area (Figure 3.37b). Numerous differences on the mass signals were observed between the normal and cancerous cells. In particular, we found that the signal at *m/z* 725 showed a massive increase in the cancerous region while the ion at *m/z* 616 almost disappeared in the cancer cells.

3.4.3.2 Visualization of Molecules Specifically Localized in Normal and Cancerous Region Having demonstrated the cancerous/normal tissue specific localization of ions at *m/z* 616 and 725, respectively, we proceed to the visualization of their distribution pattern. As expected, the ion distribution images shown in Figure 3.38 demonstrate that they are expressed in the normal/diseased region specific manner; ion at *m/z* 725 was clearly localized in the cancerous region while ion at *m/z* 616 was found only in the normal cell region. The merged image demonstrates that these two ions were complementarily distributed in the specimen.

3.4.3.3 Molecular Identification with MS/MS Next question is the origin of these two ions. As shown in previous chapters, MS/MS provides the structural information of interest ions and therefore, it enables the molecular identification. The result of MS/MS with regard to *m/z* 725 is shown in Figure 3.39A. In the product ion mass spectrum, peaks at *m/z* 666.5 and 542.5, which correspond to neutral loss (NL) of trimethylamine (59 u, C_3H_9N) and NL of trimethylamine and cyclophosphate (124 u, $C_2H_5O_4P$), respectively, were detected. This result indicates that *m/z* 725 contained an alkali metal adduct phosphocholine, therefore ion at *m/z* 725 is suggested to be PC or sphingomyelin (SM) [41]. According to the nitrogen rule, ion at *m/z* 725 having odd nominal mass should contain additional nitrogen in its structure, thus indicating presence of a sphingosine. We concluded that *m/z* 725 was attributed to be a sodiated molecule of SM (16:0).

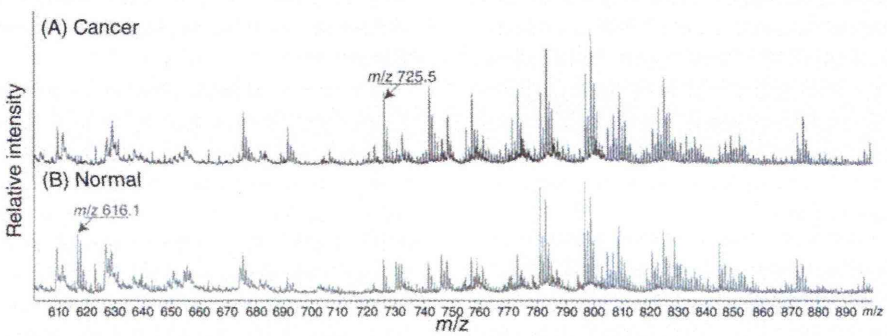

FIGURE 3.37 Comparison of averaged mass spectra from the (A) cancerous and (B) normal areas.

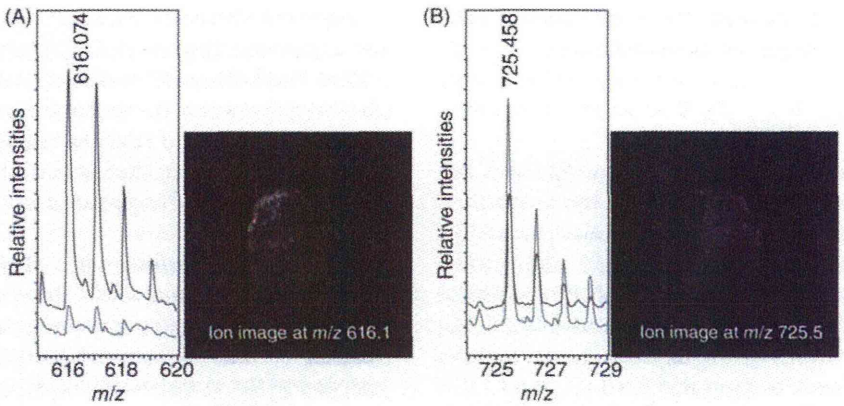

FIGURE 3.38 Visualization of molecules specifically localized in normal and cancerous region. Ion distribution images and corresponding mass spectra demonstrate the strong distribution of ion at *m/z* 616 in the normal area (A), while the ion at *m/z* 725 showed higher expression in the cancerous area than in the normal area (B).

Regarding the ion at *m/z* 616, the first generation of product ion mass spectrum from *m/z* 616 showed consecutive NLs of 73, 59, and 45 Da (Figure 3.39B[a]). From the previous literature [83,84], it is suggested that *m/z* 616 corresponded to heme B and that these NLs were derived from loss of the CH2CH2COOH (73 Da), CH2COOH (59 Da), or the COOH (45 Da) group, respectively. The molecular structure of heme B is displayed as an inset. Figure 3.39B(b) shows the second product ion mass spectrum generated from *m/z* 557, and an additional NL of 59 Da was observed. This fragment was considered to be derived from another CH2COOH in heme B.

Here, we demonstrate that SM(16:0) was strongly expressed in the cancerous area. Previous studies reported that in colon cancer, the cancerous cells contain elevated amounts of total phospholipids [85], and in addition, the phospholipid composition of the cellular membrane is altered [85,86] even between cancer cell types, that is, metastases and nonmetastatic cancer [86]. Brasitus et al. studied a relationship between the malignancy and altered lipid composition of the colon cancer, and reported significant accumulation of SM, consistent with the presented result [87]. On the other hand, heme B consists of an iron atom and porphyrin, and is known as a prosthetic group in hemoglobin, which is a protein in erythrocytes. Presented results indicate the difference between the blood-rich organ liver and the ischemic metastatic colon cancer [88,89].

3.4.3.4 IMS Linked to Multivariate Analysis Up to this point, we showed that two small metabolites were specifically expressed between the cancerous and normal tissue areas. In the described data analysis procedures without statistical methods, we usually averaged the spectra of each region and visually compared the mass peaks between the spectra one by one. As seen in Figure 3.37, with such visual comparisons of spectra, we were certainly able to find differences among the peak expressions. However, such methodology is inefficient especially when one is analyzing a large number of mass peaks and/or many tissue samples.

Below, we will describe the IMS-linked PCA to compare the metabolite composition of the normal/cancerous regions. Here, we will not describe the detailed mathematical theory due to the space limitation, but in brief, PCA is a statistical method that merges the data containing multiple elements into low-dimensional data. It reduces a large set of variables to a small set of variables called "principal components" which are linear combinations of the original variables. In the PCA-coupled IMS data analysis, spectra obtained by IMS are processed to peak detection and based on the generated peak list, PCA decomposition was performed. PCA images (i.e., 2D intensity map of principle component score on the tissue section) were often utilized to find differences of molecular composition among regions/tissues.

PCA calculation results in several parameters and below, the *component score* and *factor loading* are particularly important for the interpretation of results. A component score is calculated for each mass spectrum; all are defined for each principal component (e.g., for PC1, PC2, etc.). Those component scores are often plotted two-dimensionally, to facilitate interpretation of the PCA results. In Figure 3.40, component scores for each principle component are plotted on the *x*- and *y*-axis, and each dot in the graph represents a spectrum